Published by
NIGERIAN SOCIETY OF PHYSICAL SCIENCES
Available online @ https://asr.nsps.org.ng/index.php/asr

African Scientific Reports 5 (2026) 517

African Scientific Reports

Investigating chaos in solar activity over six solar cycles

Grace Adagba[a], Emmanuel Vezua Tikyaa[b,*], Tertsea Igbawua[b], Moses Owoicho Audu[b]

[a]Department of Physics, Moses Orshio Adasu University, Makurdi, Benue State, Nigeria
[b]Department of Physics, Joseph Sarwuan Tarka University, Makurdi, Benue State, Nigeria

Abstract

In this work, nonlinear dynamical characterization of selected geospace variables was undertaken by analyzing temporal chaotic trends in daily sunspot number (SSN), equivalent planetary amplitude (A_p), and solar radio flux ($F10.7_{\rm obs}$) data over six solar cycles (19–24). The nonlinear analysis tools used were correlation dimension, Lyapunov exponents, approximate entropy, and the Gottwald–Melbourne 0–1 test. The results show that the Lyapunov exponents, correlation dimension, and 0–1 test values indicate the presence of low-dimensional deterministic chaos in SSN, A_p, and $F10.7_{\rm obs}$. The Lyapunov exponent values were positive, the correlation dimension values fell within the range $2.1 < D_2 < 2.3$, the surrogate significance test returned positive values for all three parameters, and the 0–1 test results were very close to one (all > 0.99). The Hurst values were between 0.8 and 1, indicating persistence and long-term autocorrelation. Based on the correlation dimension and Lyapunov exponent values, the chaoticity was affirmed as $A_p < \mathrm{SSN} < F10.7_{\rm obs}$. Chaotic trends across the solar cycles showed that the degree of chaos in all three solar-cycle parameters increased from cycle 19 to cycle 24. This increase is attributed to small perturbations in interior plasma flow, shear in the axis of rotation, and variation in the strength and orientation of the Sun's geomagnetism, which are amplified over time, as evident in the decrease in the mean SSN (129–49) and increase in the signal-to-noise ratio (0.84–0.96). These processes lead to increased fluctuations in the amplitude and periodicity of solar activity from one solar cycle to another.

DOI:10.46481/asr.2026.5.2.517

Keywords: Solar cycle, Sunspot number, Equivalent planetary amplitude, Solar radio flux, Chaos.

Article history:
Received: 18 April 2026
Received in revised form: 27 May 2026
Accepted for publication: 05 June 2026
Available online: 02 July 2026

1. Introduction

Solar activity indicators are key parameters that depict the Sun's dynamics and provide valuable information on its periodic and nonperiodic fluctuations [1]. These indicators include sunspot number (SSN), global planetary index (K_p), equivalent planetary amplitude (A_p), solar radio flux ($F10.7$), and the disturbance storm time (Dst) index. Unveiling their dynamics and random fluctuations is crucial for modelling and prediction, as well as for determining the effects of solar activities such as geomagnetic storms on terrestrial life and technological systems [2, 3]. Observations over the years have shown that solar activity dynamics exhibit quasi-periodicity on multiple timescales, with a complete cyclic duration of about 11 years, defined by increases and decreases in SSN [4, 5]. SSN measures the number and distribution of sunspots on the Sun's surface and acts as a primary indicator of solar

*Corresponding author: Tel. No.: +2347032096960;
Email address: evtikyaa@uam.edu.ng (Emmanuel Vezua Tikyaa)

magnetic activity because sunspots are generated by powerful magnetic fields originating from the Sun's interior [6]. A larger SSN indicates increased magnetic disturbances on the Sun, often leading to increases in solar activity such as solar flares, coronal mass ejections (CMEs), solar radiation, and geomagnetic storms. These phenomena affect space weather in the Earth's magnetosphere and ionosphere and can disrupt satellite communications, navigation systems, and power grids.

The equivalent planetary amplitude A_p is a solar indicator that measures geomagnetic activity and represents the average disturbance level of solar particle radiation in the Earth's magnetic field. It is computed by converting the 3-hour K_p values, which range from 0 to 9, to a linear scale in nanoteslas ranging from 0 to 400 to obtain the ap values using a standard mapping table, and then taking the arithmetic mean of the eight ap values obtained for each day [7]. Larger A_p values indicate geomagnetic disturbances or storms [8]. Solar radio flux quantifies the intensity of radio emissions from the Sun, specifically in the microwave and radio wavelength range [9]. It is measured from a 100-MHz-wide band centered at 2800 MHz (10.7 cm wavelength) and recorded in solar flux units (sfu), where 1 sfu = 10^{-22} W m^{-2} Hz^{-1}. The solar flux index represents electromagnetic emissions directly linked to solar magnetic activity and supplies important real-time data about solar flares and geomagnetic storms. Monitoring fluctuations in solar radio flux is therefore important for analyzing the effects of solar activities on satellite-based telecommunication and navigation systems [10].

A considerable body of work has characterized monthly solar activity indicators using nonlinear dynamical methods, but fewer studies have used daily values. Veronig *et al*. [11] analyzed time series of different solar radio events (type I, type IV, and spikes) to unveil the nature of their underlying generating processes using nonlinear dynamics. The Grassberger–Procaccia method was applied to estimate the correlation dimension of possible attractors in stationary subsets. Most samples did not show low dimensionality, indicating stochasticity, while only two overlapping subsets of similar type IV events with spikes exhibited finite dimensions ($D_2 \sim$ 3.5 and 3.7). This variation calls for more detailed analysis of solar radio events to provide a more consistent interpretation. Mundt *et al*. [12] analyzed chaos in sunspot cycles from January 1749 to May 1990 by reconstructing the attractor in sunspot data series and computing the information dimension (D_I), correlation dimension (D_c), and largest Lyapunov exponent of the underlying system. Their results showed low-dimensional chaos in the sunspot cycles, with $D_c \approx D_I \approx 2.3$ and $\lambda_1 \approx 0.02$ month^{-1}.

Greenkorn [13] carried out nonlinear analysis of daily SSN from solar cycles 10 to 23 to determine whether convective turbulence is stochastic or chaotic. The chaotic quantifiers used included phase-space reconstruction, correlation dimension, and Lyapunov exponents for each solar cycle. The results revealed stochastic dynamics in cycles 10–19 and evolution toward chaotic dynamics in cycles 20–23. The transitions in cycles 20–23 may be due to variations in the magnitude of turbulence in the convection zone, which result in deviations in convective heat transfer and in the span of the convection region for the later cycles.

Qi-Xiu Li and Ke-Jun Li [14] characterized the monthly smoothed group sunspot number (R_g) and observed that the solar activity underlying the R_g time series is governed by a low-dimensional chaotic attractor. The maximal Lyapunov exponent (MLE) of the R_g series was positive and approximately 0.0187 ± 0.0023 month^{-1}. This implied that the predictability time of the chaotic group sunspot number is about 4.46 ± 0.5 years, which differed slightly from the predictability time obtained from the Wolf sunspot number. Both results indicate that solar activity can be forecast accurately only on a short- to medium-term basis because of its intrinsic complexity. Selvi and Selvaraj [15] investigated the chaotic nature of SSN data using nonlinear analysis techniques, including average mutual information and false nearest neighbors to obtain the time lag and embedding dimension for phase-space reconstruction, correlation dimension, and maximal Lyapunov exponent. Their results showed that the dynamical behavior of SSN is a low-dimensional chaotic attractor, with a correlation dimension of 1.98 and a maximal Lyapunov exponent of 0.337258 month^{-1}, indicating deterministic chaos rather than stochasticity. Xiao *et al*. [16] implemented the binary 0–1 test on monthly mean relative sunspot time series from January 1749 to December 2014 and observed inherently chaotic characteristics because the output of the 0–1 test was close to 1 (about 0.9885). The largest Lyapunov exponent further confirmed the presence of chaos, with positive values for embedding dimensions 5 and 6.

Ogunjo *et al*. [17] investigated dynamical complexities in geospace by characterizing the chaotic properties of hourly Dst values over four solar cycles (20–23), spanning 1964–2008, using nonlinear techniques such as sample entropy, Lyapunov exponents, correlation dimension, recurrence quantification analysis, and multifractal detrended fluctuation analysis. Geospace was observed to be chaotic in all solar cycles considered because all had positive Lyapunov exponents. The increasing order of complexity based on correlation dimension and recurrence rate values was cycle $21 < 22 < 23 < 20$. It was also observed that solar cycle 20, which has the highest mean SSN of 651.62 and standard deviation of 1656.90, has the least chaoticity, with a Lyapunov exponent of 0.004 day^{-1}. Gonçalves [18] applied an empirical method from chaos theory focused on stochastic chaos and deployed topological machine-learning algorithms to analyze sunspot data for attractor reconstruction and data-dynamics decomposition. The analysis revealed three low-dimensional chaotic attractors: a dominant attractor corresponding to a highly persistent process that exhibits self-organized criticality and multifractal patterns, a second attractor corresponding to anti-persistent multifractal patterns due to intermittent turbulence, and a third process with an ARIMA(1,0,1) signature and an independent and identically distributed noise component.

Thus, in this work, the dynamics of three solar activity variables (SSN, A_p, and $F10.7_{\text{obs}}$) are investigated to reveal inherent chaotic features. This work is novel because these three solar parameters have not been analyzed nonlinearly in a concurrent manner; therefore, the outcome is important for improved modelling and prediction of solar activity and its impact on the Earth-space climate and terrestrial telecommunication networks.

2. Nonlinear analysis

The tools of nonlinear analysis used to characterize the solar-cycle parameters in this work include phase-space reconstruction, correlation dimension, Lyapunov exponents, approximate entropy, the Hurst exponent, and the 0–1 test.

2.1. Reconstruction of phase space

This procedure involves unveiling a multidimensional embedded system, called state or phase space, from a single time series. Consider a single time series $\{s_1, s_2, \ldots, s_N\}$. Its attractor can be reconstructed into an m-dimensional phase space from delayed coordinates in the form [19, 20]

$$S_n = \left[s_n, s_{n+\tau}, s_{n+2\tau}, \ldots, s_{n+(m-1)\tau}\right]. \tag{1}$$

Here, τ is the time delay and m is the embedding dimension. The time delay τ is determined using the average mutual information (AMI) method [21]. The delay time value of the time series is the lag length at the first local minimum of the AMI plot. The embedding dimension, m, is evaluated using the false nearest neighbors (FNN) method developed by Kennel *et al.* [22]. This method involves plotting the percentage of FNN against increasing values of the embedding dimension, resulting in a monotonically decreasing curve; the minimum embedding dimension is obtained from the point at which the percentage of FNN drops to a minimum value.

2.2. Correlation dimension

Correlation dimension estimates the degrees of freedom required to model the dynamics of a system and can also be used as a quantitative tool to distinguish deterministic chaos from random noise [23]. The Grassberger–Procaccia algorithm is often applied to evaluate the correlation dimension of a data set. For a given set of reconstructed points M in an m-dimensional state space, the correlation integral $C_m(r)$ is computed as [24]

$$C_m(r) = \lim_{N\to\infty} \frac{2}{N(N-1)} \sum_{i=1}^{M} \sum_{j=i+1}^{M} \Theta\left(r - \left\|\vec{x}_i - \vec{x}_j\right\|\right), \tag{2}$$

where $\Theta(x)$ is the Heaviside function, $\|\cdots\|$ is the Euclidean norm, and r is the scaling parameter. The correlation-integral power law for small values of r has the form [24]

$$C(r) \approx r^{D_2}. \tag{3}$$

Taking the natural logarithm of both sides of Eq. (3), the correlation dimension D_2 is expressed as

$$D_2 = \lim_{r\to 0} \lim_{M\to\infty} \frac{\log C(r)}{\log r}. \tag{4}$$

A log–log plot of the correlation integral against a range of values of the neighborhood radius r yields an estimate of D_2 as the gradient of the linear part. The value of D_2 for a stochastic process is infinite, whereas for a chaotic system it is finite and fractional [25]. The significance of the correlation-dimension values was also examined to distinguish nonlinearity (deterministic chaos) from noise in the analyzed time series using surrogate data. The level of significance, S, of the difference is obtained from [26, 27]

$$S = \frac{\langle D_s \rangle - D_o}{\sigma_s}, \tag{5}$$

where D_o is the correlation dimension of the original data and $\langle D_s \rangle$ and σ_s are the mean and standard deviation of the correlation dimensions of five surrogate data sets generated using the amplitude-adjusted Fourier-transform technique. A positive value of S indicates chaos and confirms nonlinearity.

2.3. Lyapunov exponent

The Lyapunov exponent, λ, characterizes the rate of separation of infinitesimally close trajectories. It is computed as [28]

$$\lambda_1(i) = \frac{1}{i\Delta t} \frac{1}{M-i} \sum_{j=1}^{M-i} \ln \frac{d_j(i)}{d_j(0)}. \tag{6}$$

Here, Δt is the sampling interval, $d_j(i)$ is the distance between the jth pair of nearest neighbors after i discrete-time steps, $d_j(0)$ is the initial separation of nearest neighbors, and M is the number of reconstructed phase-space points. A positive Lyapunov exponent indicates chaotic behavior, whereas a negative value indicates periodic behavior [27]. In this work, Rosenstein's algorithm was implemented to compute the largest Lyapunov exponent of the solar parameters [29].

2.4. Approximate entropy

Approximate entropy quantifies random fluctuations and complexity in a time series [30]. It is used to estimate the degree of complexity and information loss in a data set. The approximate entropy, Φ, is computed from

$$\Phi = \Phi_m - \Phi_{m+1}, \tag{7}$$

and

$$\Phi_m = (M - m + 1)^{-1} \sum_{i=1}^{N-m+1} \log(M_i). \tag{8}$$

Here, m is the embedding dimension and M is the number of reconstructed phase points in m-dimensional state space. Higher values of approximate entropy reflect a greater likelihood that similar patterns of observations are not followed by additional similar observations [28].

2.5. Hurst exponent

The Hurst exponent estimates the long-term memory of the data set. In this work, rescaled-range analysis was used to compute the Hurst exponent [31]. The Hurst exponent, H, is defined by the asymptotic behavior of the rescaled range as a function of the time span of the series [32]:

$$E\left(\frac{R(n)}{S(n)}\right) = \lim_{n\to\infty} Kn^H, \tag{9}$$

where $R(n)$ is the range of the first n values, $S(n)$ is the standard deviation, $E[\cdot]$ is the expected value, n is the number of data points in the time series, and K is a constant. According to Kriz [33], $0 < H < 0.5$ indicates an anti-persistent time series, $0.5 < H < 1$ indicates a persistent time series with long-term positive autocorrelation and predictability, and $H = 0.5$ implies Brownian motion or random walk.

2.6. Gottwald–Melbourne 0–1 test

The 0–1 test is a binary test for chaos that is applied directly to the time series. Given a one-dimensional set of data points $\phi(i)$ for $i = 1, \ldots, N$ and a real parameter $c \in (0, \pi)$, the translation variables $p_c(n)$ and $q_c(n)$ are computed as [34]

$$p_c(n) = \sum_{i=1}^{n} \phi(i) \cos ic, \tag{10}$$

and

$$q_c(n) = \sum_{i=1}^{n} \phi(i) \sin ic, \tag{11}$$

where $n = 1, 2, 3, \ldots, N$.
Next, the growth of $p_c(n)$ and $q_c(n)$, the smoothed mean square displacement (MSD) is then computed:

$$M_c(n) = \lim_{N\to\infty} \frac{1}{N} \sum_{i=1}^{N} \left[(p_c(i+n) - p_c(i))^2 + (q_c(i+n) - q_c(i))^2 \right]. \tag{12}$$

The chaos test is based on the asymptotic growth rate, K_c, of $M_c(n)$ with respect to n. This is achieved by computing the MSD values $\Delta = M_c(\xi)$ for different values of $\xi = 1, 2, 3, \ldots, n$. The asymptotic growth rate, K_c, is then determined by computing the correlation coefficient of ξ and Δ for different values of c, such that

$$K_c = \mathrm{corr}(\xi, \Delta) = \frac{\mathrm{cov}(\xi, \Delta)}{\sqrt{\mathrm{var}(\xi)\mathrm{var}(\Delta)}}. \tag{13}$$

The median value is regarded as the output of the 0–1 test, K_{median}. The output of this test lies between 0 and 1, with values closer to 1 indicating chaoticity and values closer to 0 indicating nonchaotic or regular behavior [27]. Intermediate values, for example in the neighborhood of 0.5, can indicate partial or weak chaos (quasi-chaoticity), as observed in systems such as the logistic map [35].

Table 1: Duration and descriptive statistics of solar sunspot numbers (SSN) across different solar cycles.

Solar cycle	Period (time span)	Duration (year–months)	Mean SSN	Standard deviation	SNR	Maximum SSN	Zero-sunspot days
19	April 1954–September 1964	10–6	129	109	0.845	503	337
20	September 1964–February 1976	11–5	86	63	0.733	304	303
21	February 1976–September 1986	10–6	110	92	0.836	428	319
22	September 1986–August 1996	9–11	106	87	0.821	410	257
23	August 1996–December 2008	12–4	82	73	0.890	353	647
24	December 2008–December 2019	11–0	49	47	0.959	220	942

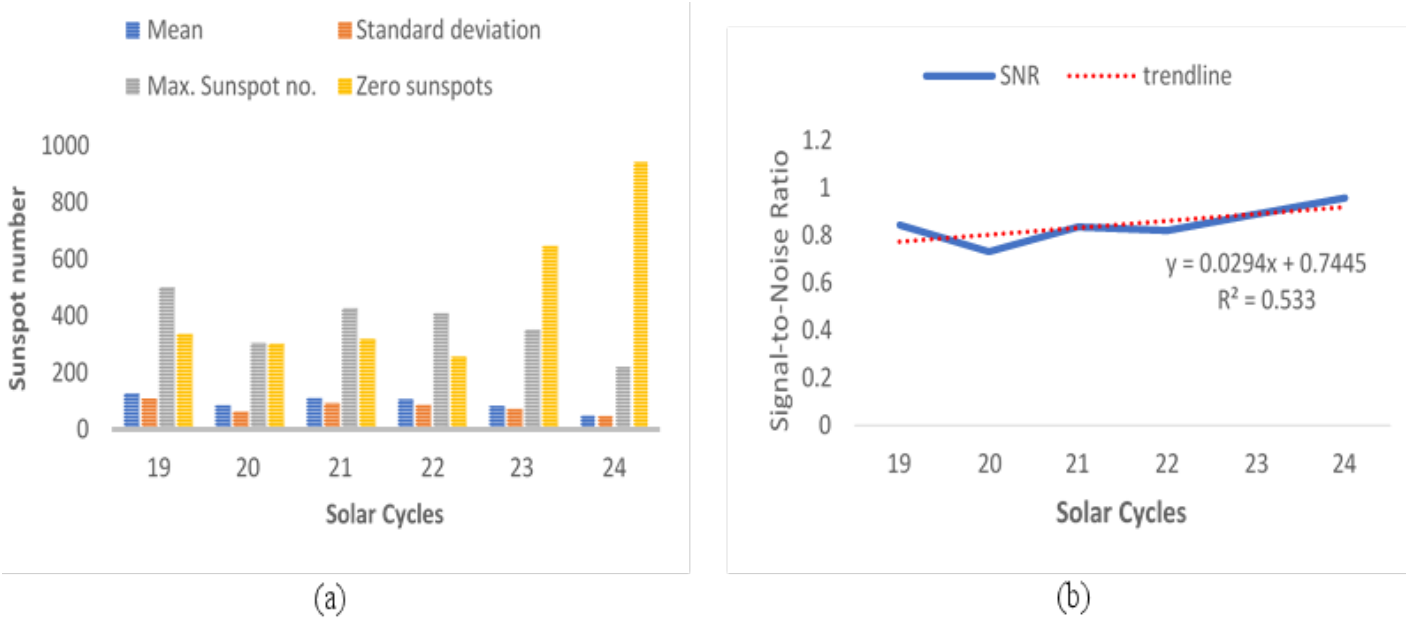

Figure 1: Descriptive statistics of solar sunspot numbers from solar cycles 19–24.

Table 2: Descriptive statistics of equivalent planetary amplitude and solar radio flux across different solar cycles.

Solar cycle	Mean A_p	SD A_p	SNR A_p	Mean $F10.7_{\text{obs}}$	SD $F10.7_{\text{obs}}$	SNR $F10.7_{\text{obs}}$
19	16.046	19.352	0.829	136.987	67.854	2.019
20	12.741	13.461	0.947	113.963	35.297	3.229
21	15.319	16.436	0.932	110.097	35.776	3.077
22	15.462	16.363	0.945	133.332	59.487	2.241
23	12.061	14.350	0.841	119.383	51.087	2.337
24	7.887	8.176	0.965	97.817	33.052	2.959
Overall	13.212	15.102	0.875	123.141	53.846	2.287

3. Data source and pre-processing

The solar and geomagnetic index data used in this work were sourced from the GFZ Helmholtz Centre for Geosciences, Potsdam, Germany [36]. The data were characterized using standard indices and include daily values of SSN, $F10.7_{\text{obs}}$, which is the 10.7-cm solar radio flux observed at 10.7 cm, and A_p or the geomagnetic K_p index. The data span 1 January 1964 to 31 December 2019, covering six solar cycles (19–24) [37]. The duration and descriptive statistics of SSN across the different cycles are presented in Tables 1 and 2, and the SSN statistics are displayed in Figure 1 [36, 38, 39].

Before evaluating the chaotic quantifiers, trends and cyclic components (seasonal variations) were removed from the data by seasonal differencing, rendering the data stationary, with zero mean and constant variance of unity. This procedure reveals the deterministic components and noise in the data, which were then analyzed [40].

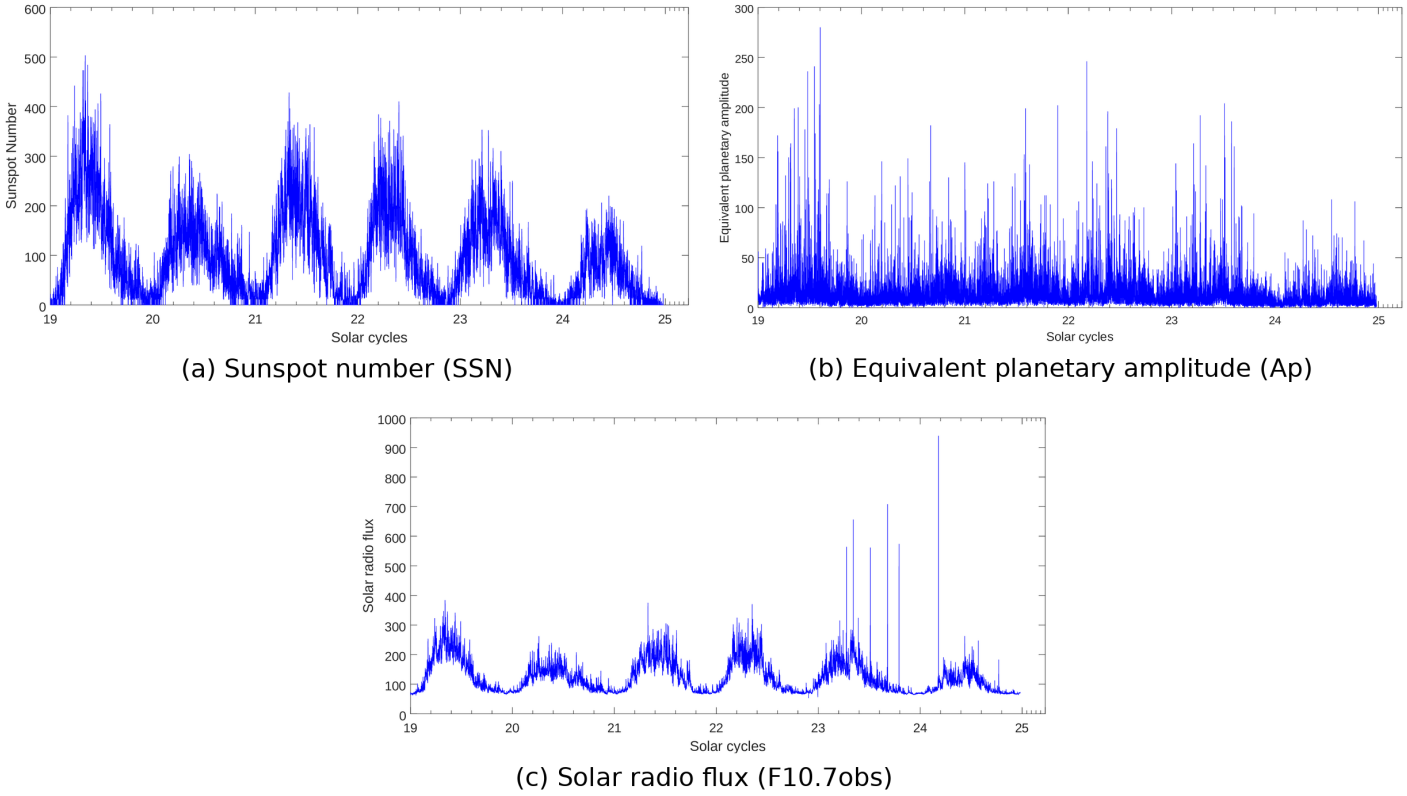

Figure 2: Time series of daily values of solar activity parameters from solar cycles 19–24.

Table 3: Computed nonlinear parameters (chaotic quantifiers) for the solar-cycle parameters.

Parameter	τ	m	λ (day^{-1})	D_2	S	ϕ	H	0–1 test
SSN	10	4	0.00624	2.212	0.938	0.984	0.996	0.9979
A_p	7	2	0.00151	2.172	1.868	1.481	0.847	0.9977
$F10.7_{\text{obs}}$	10	4	0.00932	2.184	2.668	0.761	0.989	0.9988

4. Results and discussion

4.1. Solar-cycle parameter plots

The time series of the daily values of the solar-cycle parameters analyzed in this work from solar cycles 19–24 are presented in Figure 2.

The magnetic field of the Sun is generated by the solar dynamo, which manifests in the convection zone and solar tachocline. Differential rotation, which is more rapid at the solar equator than at the poles, twists and stretches the magnetic flux into a toroidal east–west configuration, leading to the eruption of sunspots. Variations in sunspots and other solar parameters result from the sensitive dependence of the strength and organization of the toroidal field on the quantity of magnetic flux that carries over from the preceding solar cycle, as well as its latitudinal and depth-wise distribution [41]. The time-series plots of the solar-cycle parameters in Figure 2 exhibit irregular, aperiodic, or unpredictable behavior that may be described as either random or chaotic. On the other hand, the oscillations evolve through cycles of approximately 11 years in a quasiperiodic manner; that is, they are roughly periodic but not perfectly regular. This behavior may result from small perturbations in interior plasma flow, shear in the axis of rotation, and magnetic-flux transfer, which are amplified over time (the butterfly effect), leading to variations in the amplitudes, duration, and spatial patterns of activity in successive solar cycles [42].

4.2. Nonlinear characterization of solar-cycle parameters

The results of the overall characterization of the three solar-cycle parameters using chaotic quantifiers such as Lyapunov exponents (λ), correlation dimension (D_2), approximate entropy (ϕ), Hurst exponent (H), and the 0–1 test (K_{median}) are presented in Table 3.

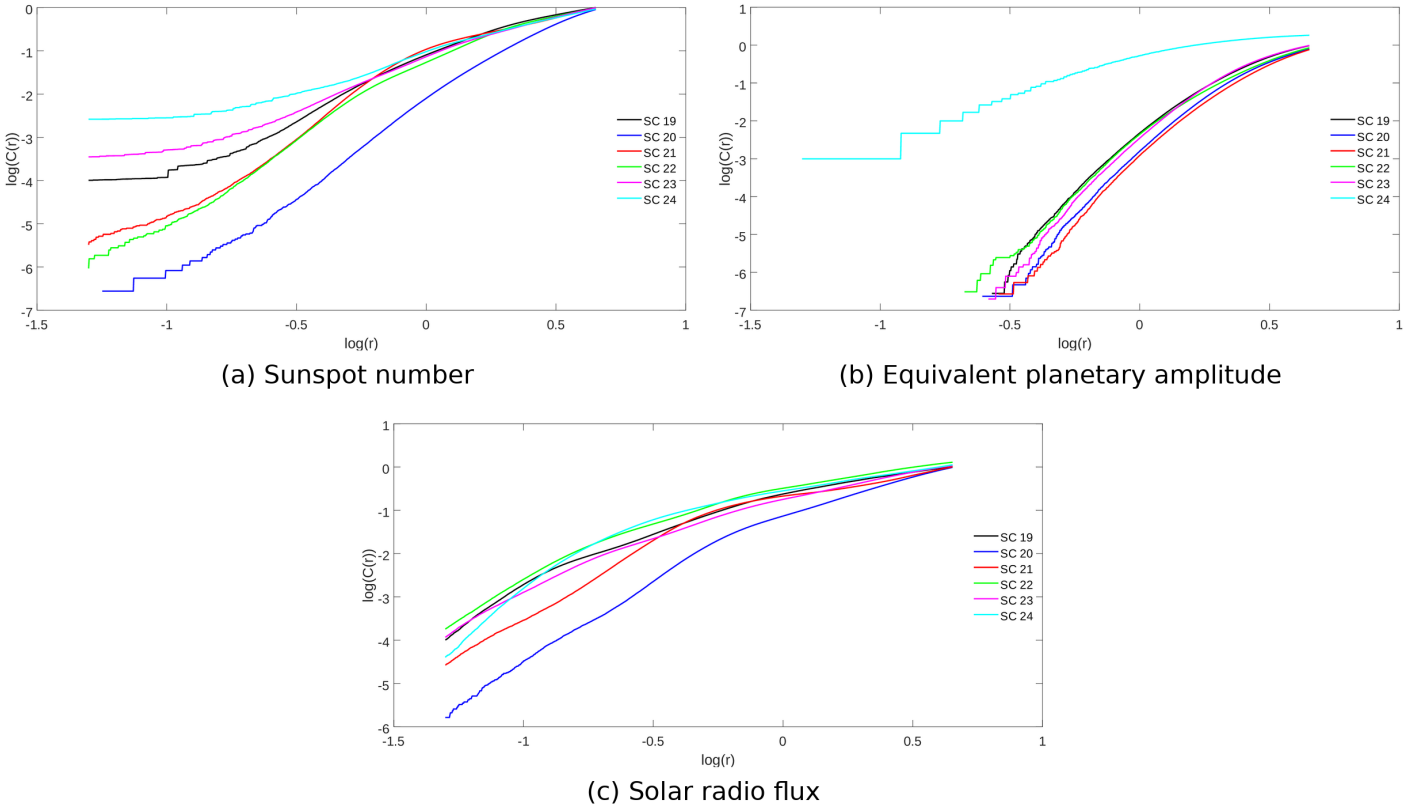

Figure 3: Analysis of correlation dimension for (a) sunspot number, (b) equivalent planetary amplitude, and (c) solar radio flux from solar cycles 19–24.

From the results in Table 3, the Lyapunov exponents, correlation dimensions, and 0–1 test results indicate the presence of low-dimensional deterministic chaos in SSN, A_p, and $F10.7_{\text{obs}}$. The Lyapunov exponent values are all positive, and the correlation-dimension values fall within the range $2.1 < D_2 < 2.3$, agreeing with Refs. [14–16]. While SSN and $F10.7_{\text{obs}}$ have similar time-delay (τ) and embedding-dimension (m) values of 10 and 4, respectively, A_p has lower values of τ and m, namely 7 and 2. A_p also recorded the lowest Lyapunov exponent and correlation dimension values (0.001509 and 2.172) compared with SSN and $F10.7_{\text{obs}}$. The correlation-dimension surrogate test returned positive values for all three parameters, while the 0–1 test returned values close to one (all > 0.99), confirming the presence of chaos in the data sets of the solar-cycle parameters. $F10.7_{\text{obs}}$ appears to be more chaotic because it has the highest Lyapunov exponent and 0–1 test statistic. In terms of the degrees of freedom and chaos in the data sets, the order was $A_p < \text{SSN} < F10.7_{\text{obs}}$. This implies that systems with higher correlation-dimension values exhibit greater complexity because they require more variables for modelling. Similarly, the Hurst values, which lie between 0.8 and 1, indicate persistence in all three solar-cycle parameters, implying long-term autocorrelation and predictability of the time series. However, the approximate entropy values are all below 1, indicating a low rate of information loss in the solar-cycle parameters.

4.3. Trend of dynamical complexity in the solar-cycle parameters across solar cycles

The chaotic quantifiers were computed for all three solar-cycle parameters from solar cycles 19–24, and the results of the analysis are presented in Figures 3 and 4. The temporal variations in the chaotic quantifiers for the different parameters across the six solar cycles are presented in Tables 4–6, while the trend plots are presented in Figures 5–7.

The results in Table 4 and Figure 5 show the computed chaotic quantifiers for SSN and their trends from solar cycles 19–24. The Lyapunov exponents for SSN were all positive, indicating deterministic chaos in all solar cycles, with cycle 20 having the maximum value of 0.01398 day^{-1} and cycle 24 having the minimum value of 0.004665 day^{-1}. This implies that SSN for cycle 20 is predictable for the next 71.5 days, while that for cycle 24 is predictable for the next 214.4 days. The degree of chaos was ranked in ascending order as cycle 24 < cycle 22 < cycle 19 < cycle 21 < cycle 23 < cycle 20, and a weak decreasing trend in Lyapunov exponents was observed from cycle 19 to cycle 24, with $R = -0.4101$ and a negative trendline slope. The correlation dimensions for SSN were low (< 4), indicating a low degree of complexity, with cycle 20 having the maximum value of 3.6507 and cycle 24 having the minimum value of 1.6086. The degree of complexity in SSN was ranked in ascending order as cycle 24 < cycle 23 < cycle 19 < cycle 21 < cycle 22 < cycle 20, and a strong decreasing trend in D_2 was observed from cycle 19 to cycle 24, with $R = -0.6263$. The significance values, S, for D_2 using five surrogate data sets were positive for all solar cycles, affirming chaos and nonlinearity.

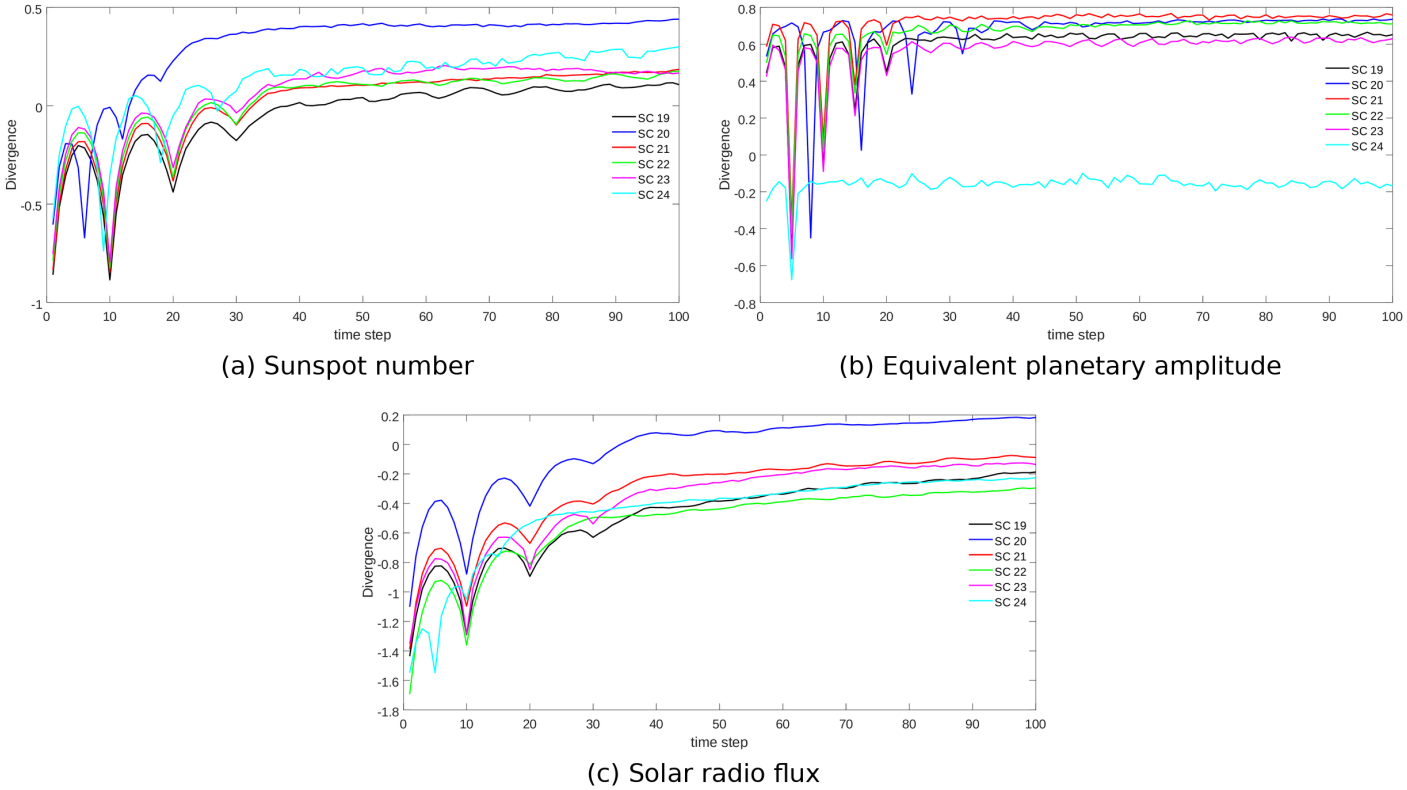

Figure 4: Analysis of Lyapunov exponent for (a) sunspot number, (b) equivalent planetary amplitude, and (c) solar radio flux from solar cycles 19–24.

Table 4: Chaotic quantifiers for sunspot number (SSN) across the solar cycles.

Cycle	τ	m	λ (day^{-1})	D_2	S	ϕ	H	0–1 test
19	10	4	0.00525	2.556	0.0767	0.6400	0.882	0.9476
20	6	4	0.01398	3.651	0.9852	0.6235	0.808	0.9888
21	10	4	0.00574	3.225	0.1710	0.6138	0.802	0.9702
22	10	4	0.00502	3.313	1.5746	0.6159	0.796	0.9661
23	10	4	0.00609	2.146	2.8729	0.6182	0.825	0.9837
24	9	4	0.00467	1.609	0.7912	0.6035	0.934	0.9920

Furthermore, the approximate entropy values for SSN were low (< 1), indicating a minimal degree of repetitive patterns and information loss, with cycle 19 having the maximum value of 0.64 and cycle 24 having the minimum value of 0.6035. The degree of repetitive patterns in SSN cycles was ranked in ascending order as cycle 24 < cycle 21 < cycle 22 < cycle 23 < cycle 20 < cycle 19, while a strong decreasing trend was observed from cycle 19 to cycle 24, with $R = -0.8632$. The Hurst exponent values for SSN were all greater than 0.5, indicating persistence in the SSN time series. Cycle 24 had the maximum persistence of 0.9343, while cycle 22 had the minimum persistence of 0.7961. The degree of persistence in SSN cycles was ranked in ascending order as cycle 22 < cycle 21 < cycle 20 < cycle 23 < cycle 19 < cycle 24, while a very weak increasing trend in H was observed from cycle 19 to cycle 24, with $R = 0.2963$. The 0–1 test results all showed values close to 1, indicating chaos, with cycle 24 having the maximum value of 0.992 and cycle 19 having the minimum value of 0.9476. The degree of chaos based on the 0–1 test was ranked as cycle 19 < cycle 22 < cycle 21 < cycle 23 < cycle 20 < cycle 24.

The results in Table 5 and Figure 6 show the computed chaotic quantifiers for A_p and its trends from solar cycles 19–24. The Lyapunov exponents for A_p were positive, indicating deterministic chaos. Based on the values in Table 5, cycle 24 has the maximum value of 0.004138 day^{-1}, while cycle 20 has the minimum value of 0.001828 day^{-1}. This implies that A_p for cycle 20 is predictable for about 547 days, while that for cycle 24 is predictable for about 242 days. The degree of chaos in A_p is ranked in ascending order as cycle 20 < cycle 21 < cycle 23 < cycle 19 < cycle 22 < cycle 24, and an increasing trend in Lyapunov exponents was observed from cycle 19 to cycle 24, with $R = 0.6872$. The correlation dimensions for A_p were greater than 5, indicating a higher degree of complexity, with cycle 20 having the maximum value of 5.86 and cycle 22 having the minimum value of 5.13. The degree of

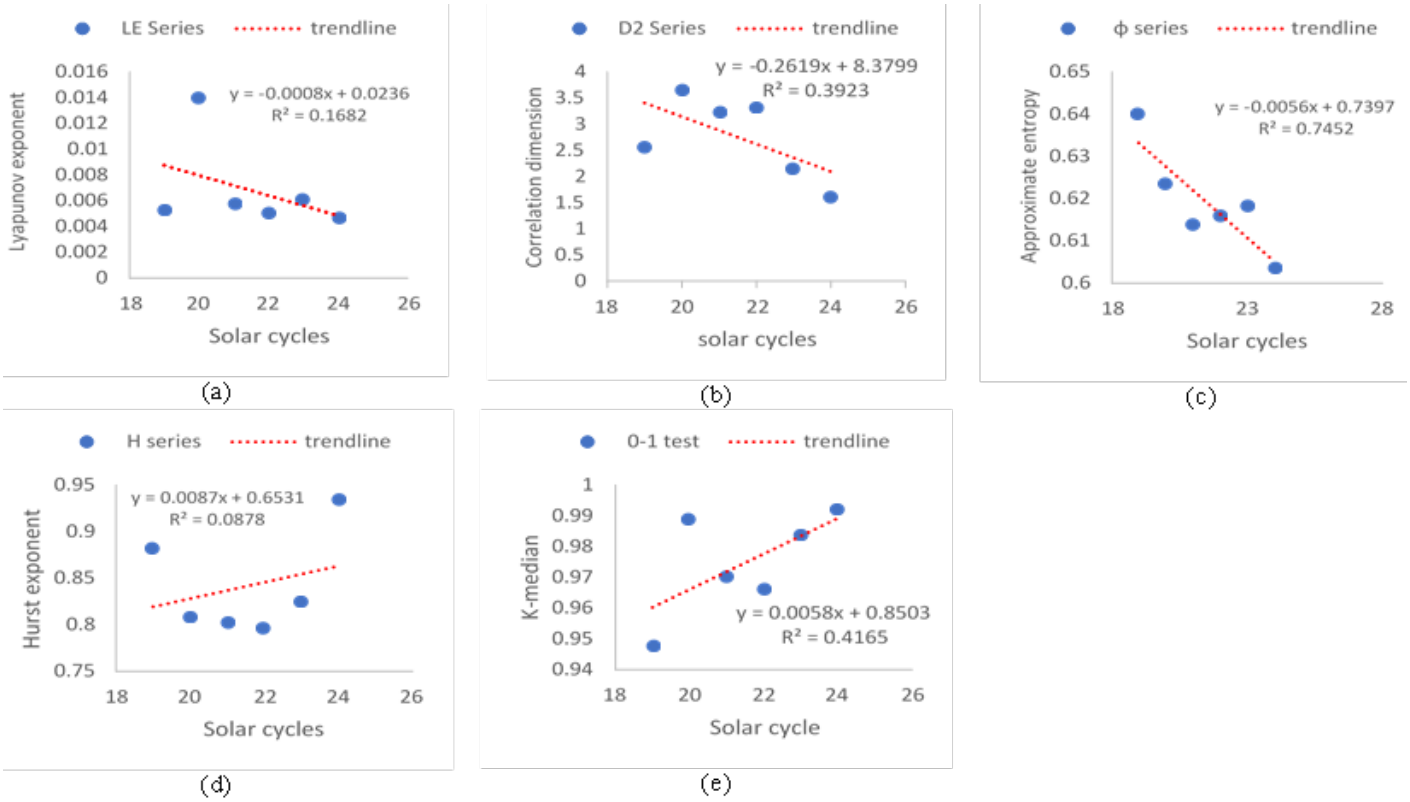

Figure 5: Trends of (a) Lyapunov exponent, (b) correlation dimension, (c) approximate entropy, (d) Hurst exponent, and (e) 0–1 test statistic K_{median} for sunspot number from solar cycles 19–24.

Table 5: Chaotic quantifiers for equivalent planetary amplitude (A_p) across the solar cycles.

Cycle	τ	m	λ (day^{-1})	D_2	ϕ	H	S	0–1 test
19	5	5	0.00209	5.236	0.5579	0.739	1.404	0.9973
20	8	5	0.00183	5.863	0.5261	0.666	-2.881	0.9982
21	5	5	0.00183	5.713	0.3881	0.704	0.743	0.9985
22	5	5	0.00219	5.132	0.5677	0.754	1.467	0.9979
23	5	5	0.00208	5.593	0.5664	0.723	-1.088	0.9973
24	5	5	0.00414	5.322	0.3659	0.611	-0.295	0.9978

complexity in A_p was ranked in ascending order as cycle 22 < cycle 19 < cycle 24 < cycle 23 < cycle 21 < cycle 20. The significance values, S, for D_2 using five surrogate data sets in cycles 19, 21, and 22 were positive, affirming chaos and nonlinearity, while those of cycles 20, 23, and 24 were negative, indicating noise and random oscillations (stochasticity).

The A_p correlation-dimension discrepancy between Tables 3 and 5 occurs because a shorter time series (individual solar cycles) can estimate a higher correlation dimension than the full series (entire solar cycles 19–24) if the segment is more complex, less periodic, or contains more noise than the overall data [43]. Correlation dimension is a scale-based estimate of the density of points in phase space and is sensitive to sample length, embedding choices, and the selected scaling range [44]. Thus, if the full time series mixes multiple regimes, a cleaner or more constrained global attractor can yield a lower estimate, while a local segment may appear more spread out and produce a higher slope in the scaling region [45]. Table 2 shows that the SNR for the overall A_p time series (0.875) is lower than that of the individual cycles, which are greater than 0.9 except for cycles 19 and 23.

Similarly, the approximate entropy values for A_p were low (< 1), indicating a low degree of repetitive patterns and information loss, with cycle 22 having the maximum value of 0.5677 and cycle 24 having the minimum value of 0.3659. The degree of repetitive patterns in A_p cycles was observed as cycle 24 < cycle 21 < cycle 20 < cycle 19 < cycle 23 < cycle 22. The Hurst exponent values for A_p were all greater than 0.5, indicating persistence in the A_p data set. Cycle 22 returned the maximum persistence of 0.754, while cycle 24 had the minimum persistence of 0.6107. The degree of persistence in A_p cycles was ranked in ascending order as cycle 24 < cycle 20 < cycle 21 < cycle 23 < cycle 19 < cycle 22. The 0–1 test results all showed values above 0.99, indicating chaos, with cycle

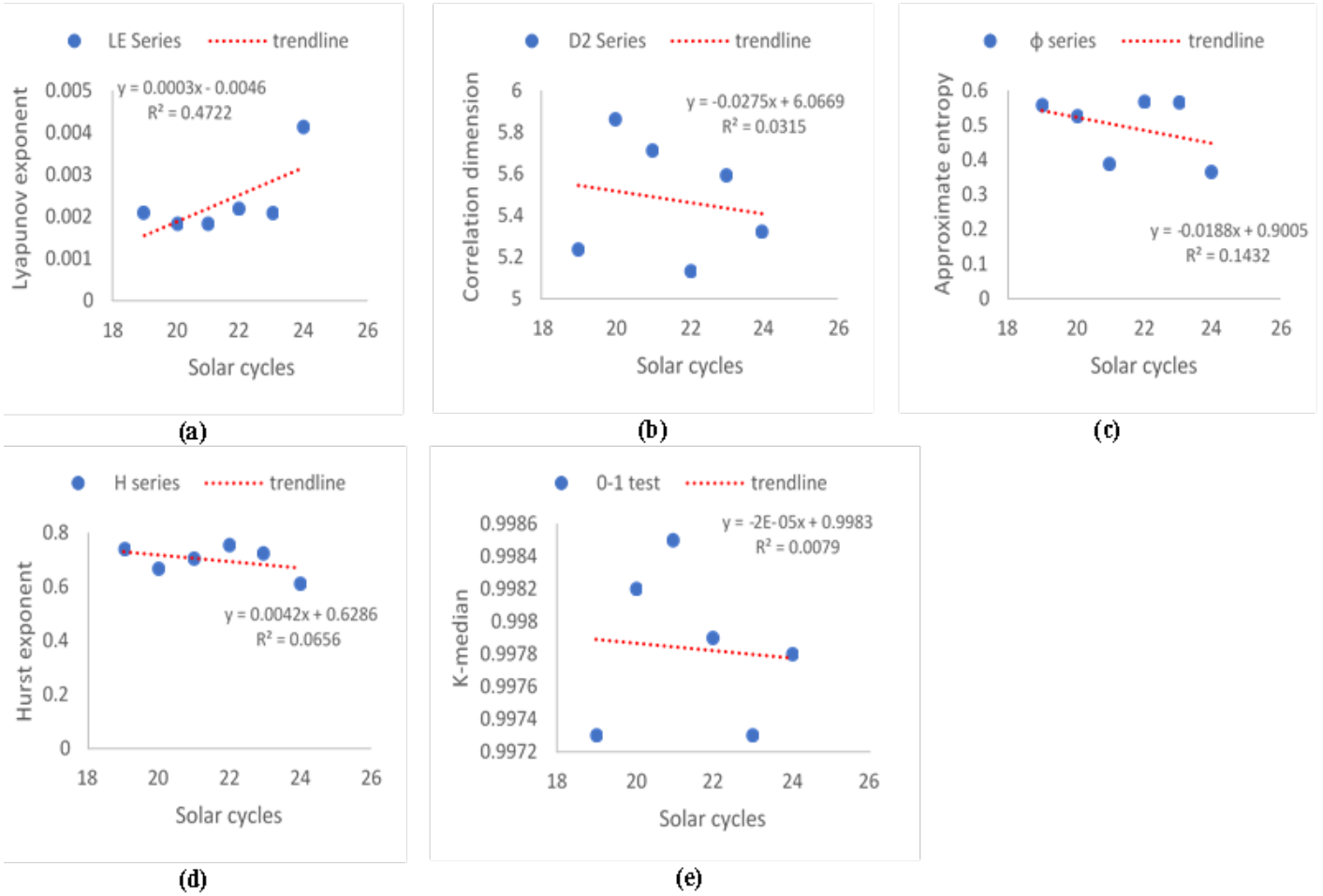

Figure 6: Trends of (a) Lyapunov exponent, (b) correlation dimension, (c) approximate entropy, (d) Hurst exponent, and (e) 0–1 test statistic K_{median} for equivalent planetary amplitude from solar cycles 19–24.

Table 6: Chaotic quantifiers for solar radio flux ($F10.7_{\text{obs}}$) across the solar cycles.

Cycle	τ	m	λ (day^{-1})	D_2	ϕ	H	S	0–1 test
19	10	4	0.00819	2.060	0.493	0.911	1.8998	0.6942
20	10	4	0.00725	2.863	0.598	0.841	1.4937	0.8676
21	10	4	0.00765	2.199	0.472	0.850	1.2913	0.6416
22	10	3	0.00733	1.688	0.758	0.871	1.4970	0.7779
23	10	4	0.00847	1.816	0.542	0.795	2.4797	0.9980
24	5	4	0.00781	1.720	0.488	0.875	2.5713	0.9993

21 having the maximum value of 0.9985 and cycles 19 and 23 having the minimum value of 0.9973. The degree of chaos based on the 0–1 test was ranked as cycles 19 and 23 < cycle 24 < cycle 22 < cycle 20 < cycle 21, with no defined trend recorded.

The nonlinear parameters for $F10.7_{\text{obs}}$ and their trends from solar cycles 19–24 are presented in Table 6 and Figure 7. The Lyapunov exponents for $F10.7_{\text{obs}}$ for all cycles are positive, indicating deterministic chaos, with cycle 23 having the maximum value of 0.008472 day^{-1} and cycle 20 having the minimum value of 0.007246 day^{-1}. This implies that $F10.7_{\text{obs}}$ for cycle 23 is predictable for about 118 days, while that for cycle 20 is predictable for about 138 days. The degree of chaos in $F10.7_{\text{obs}}$, based on the Lyapunov exponent values in Table 6, is ranked in ascending order as cycle 20 < cycle 22 < cycle 21 < cycle 24 < cycle 19 < cycle 23, and a weak increasing chaotic trend was observed from cycle 19 to cycle 24, with $R = 0.1575$. The correlation dimensions for $F10.7_{\text{obs}}$ were low (< 3), indicating a low degree of complexity, with cycle 20 having the maximum value of 2.8631 and cycle 22 having the minimum value of 1.6877. The degree of complexity in $F10.7_{\text{obs}}$ was ranked as cycle 22 < cycle 24 < cycle 23 < cycle 19 < cycle 21 < cycle 20, and a strong decreasing trend in D_2 was observed from cycle 19 to cycle 24, with $R = -0.6470$. The significance values,

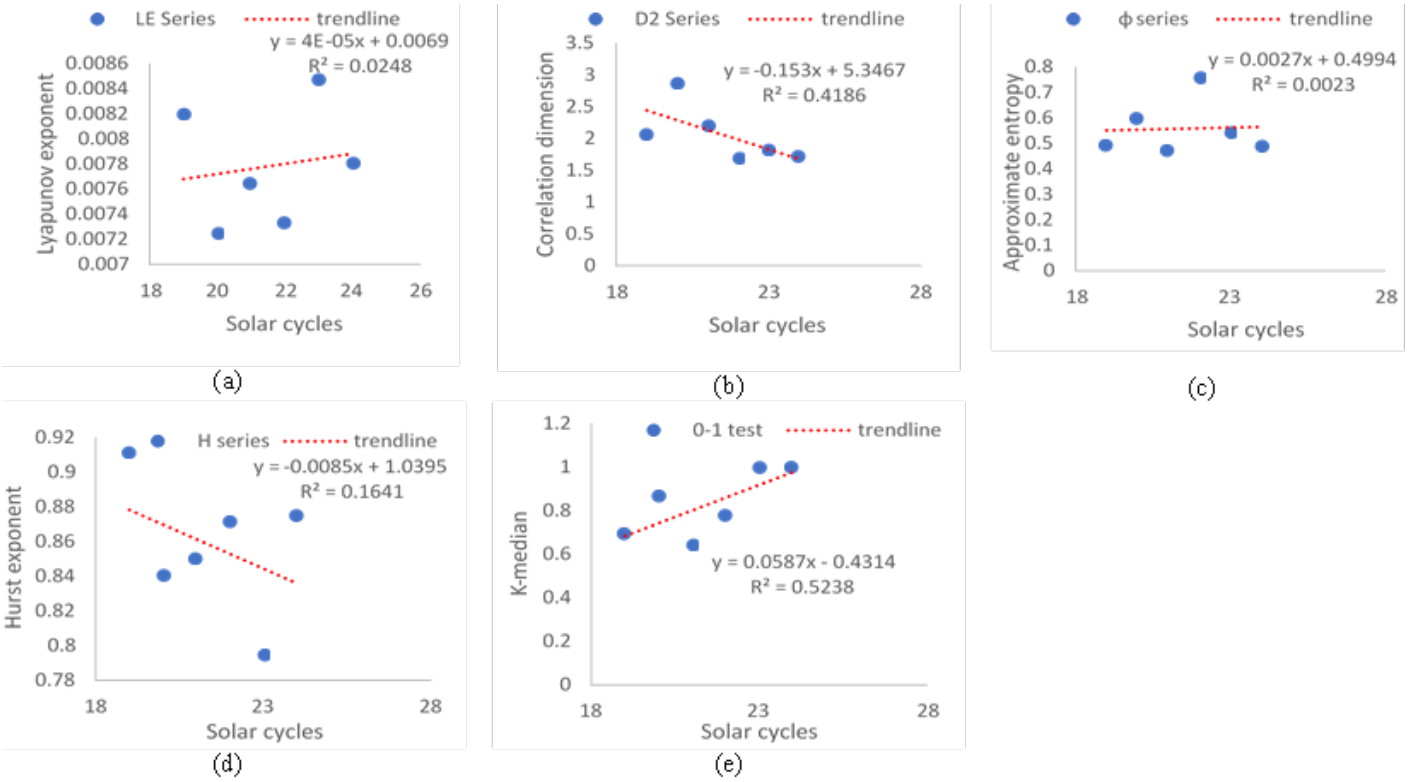

Figure 7: Trends of (a) Lyapunov exponent, (b) correlation dimension, (c) approximate entropy, (d) Hurst exponent, and (e) 0–1 test statistic K_{median} for solar radio flux from solar cycles 19–24.

S, for D_2 using five surrogate data sets were positive in all cycles, affirming chaos and nonlinearity.

Furthermore, the approximate entropy values for $F10.7_{\text{obs}}$ were low (< 1), indicating a low degree of repetitive patterns and information loss, with cycle 22 having the maximum value of 0.7577 and cycle 21 having the minimum value of 0.4716. The approximate-entropy ranking was observed as cycle 21 < cycle 24 < cycle 19 < cycle 23 < cycle 20 < cycle 22, and no significant trend in ϕ was reported from cycle 19 to cycle 24, with $R = 0.048$. Similarly, all Hurst exponent values for $F10.7_{\text{obs}}$ were greater than 0.5, affirming persistence in the $F10.7_{\text{obs}}$ time series. Cycle 19 returned the maximum persistence value of 0.9111, while cycle 23 had the minimum persistence value of 0.7946. The degree of persistence in $F10.7_{\text{obs}}$ was ranked across the cycles as cycle 23 < cycle 20 < cycle 21 < cycle 24 < cycle 22 < cycle 19, with a weak decreasing trend from cycles 19 to 24, with $R = -0.4051$. Finally, the 0–1 test results for cycles 19, 21, and 22 returned intermediate values in the neighborhood of 0.5, indicating weak chaos (quasi-chaoticity), while cycles 20, 23, and 24 returned values closer to 1, indicating chaos. The degree of chaos based on the 0–1 test was ranked as cycle 21 < cycle 19 < cycle 22 < cycle 20 < cycle 23 < cycle 24, with a strong increasing trend from cycle 19 to cycle 24 ($R = 0.7237$).

5. Conclusion

The findings of this work show that, based on the Lyapunov exponents and 0–1 test statistic, the degree of chaos follows $F10.7_{\text{obs}}$ > SSN > A_p, while the level of complexity follows SSN > A_p > $F10.7_{\text{obs}}$ based on the correlation-dimension and approximate-entropy results. Similarly, the degree of chaos in SSN increased from cycle 19 to cycle 24 based on the 0–1 test, while its level of complexity decreased; the degree of chaos in A_p increased across the cycles, while its complexity recorded no significant trend; and the degree of chaos in $F10.7_{\text{obs}}$ also increased from cycle 19 to cycle 24, while its level of complexity decreased. The increase in chaoticity and decrease in degrees of freedom may be driven by small perturbations in interior plasma flow, shear in the axis of rotation, and variation in the strength and orientation of the Sun's geomagnetism. These perturbations are amplified over time, as evident in the decrease in mean SSN (129–49) and the increase in signal-to-noise ratio (0.84–0.96), leading to increased fluctuations in the amplitude and periodicity of solar activity from one solar cycle to another.

Data availability

Data used are available from the corresponding author by request.

Declaration of competing interest

The authors declare that they have no known competing financial interests or personal relationships that could have appeared to influence the work reported in this manuscript.

Funding

This study was funded exclusively by the authors

Acknowledgment

The authors wish to acknowledge the Helmholtz Centre for Geosciences for granting access to its solar and geomagnetic indices database (https://kp.gfz.de/en/data) in the course of this work.

References

[1] S. Yamakawa, M. Inoue & R. Suppiah, "Relationships between solar activity and variations in SST and atmospheric circulation in the stratosphere and troposphere", Quaternary International **397** (2016) 289. https://doi.org/10.1016/j.quaint.2015.11.018
[2] B. Adhikari, S. Dahal, R. K. Mishra & N. Sapkota, "Analysis of solar, interplanetary, and geomagnetic parameters during solar cycles 22, 23 and 24", Russian Journal of Earth Sciences **19** (2019). https://doi.org/10.2205/2018ES000645.
[3] R. Sharma, O. P. Tripathi, A. Dwivedi & S. Kumar, "Association of sunspot number, solar radio flux and geomagnetic storms during the period of 2009–2019", International Journal of Recent Scientific Research **14** (2023) 6. https://www.researchgate.net/publication/372159241_ASSOCIATION_OF_SUNSPOT_NUMBER_SOLAR_RADIO_FLUX_AND_GEOMAGNETIC_STORMS_DURING_THE_PERIOD_OF_2009-2019
[4] D. H. Hathaway, "The solar cycle", Living Reviews in Solar Physics **7** (2010) 25. https://doi.org/10.1007/s41116-023-00037-y.
[5] R. G. Cionco, S. M. Kudryavtsev & W. W.-H. Soon, "Tidal forcing on the Sun and the 11-year solar-activity cycle", Solar Physics **298** (2023) 70. https://doi.org/10.1007/s11207-023-02167-w.
[6] S. K. Solanki, "Sunspots: An overview", Astronomy and Astrophysics Review **11** (2003) 153–286. https://doi.org/10.1007/s00159-003-0018-4.
[7] J. Matzka, C. Stolle, Y. Yamazaki, O. Bronkalla & A. Morschhauser, "The geomagnetic Kp index and derived indices of geomagnetic activity", Space Weather **19** (2021). https://doi.org/10.1029/2020SW002641.
[8] C. G. Njumogu & T. N. Obiekezie, "Selection of ten geomagnetially quietest days using Kp index", IOSR Journal of Applied Geology and Geophysics (IOSR-JAGG) **8(2)** (2020) 54. https://doi.org/10.9790/0990-0802015457.
[9] K. F. Tapping, "The 10.7 cm solar radio flux (F10.7)", Space Weather **11** (2013) 394. https://doi.org/10.1002/swe.20064.
[10] G. S. Lakhina, "Solar wind-magnetosphere-ionosphere coupling and chaotic dynamic", Surveys in Geophysics **15** (1994) 703. https://doi.org/10.1007/BF00666091.
[11] A. Veronig, M. Messerotti & A. Hanslmeier, *Nonlinear analysis of solar radio events: A preliminary approach*, Institut fur Astronomie, University of Graz, Austria, **A-8010** (1991). https://www.google.com/url?q=https://austriaca.at/0xc1aa5572%200x0015cd5b.pdf&sa=U&ved=2ahUKEwiGhrHO8ayVAxXjl1YBHV-_ImoQFnoECAoQAg&usg=AOvVaw1934YAx7P5dYSWYIAx6EWa.
[12] M. D. Mundt, W. B. Maguire II & R. P. Chase, "Chaos in the sunspot cycles: Analysis and prediction", Journal of Geophysical Research **96(A2)** (1991) 1705. https://doi.org/10.1029/90JA02150
[13] R. A. Greenkorn, "Analysis of sunspot activity cycles", Solar Physics **255** (2009) 301. https://doi.org/10.1007/s11207-009-9331-z.
[14] Q.-X. Li & K.-J. Li, "Low dimensional chaos from the group sunspot numbers", Chinese Journal of Astronomy and Astrophysics **7(3)** (2007) 435. Available online: https://doi.org/10.1088/1009-9271/7/3/14.
[15] S. T. Selvi & R. S. Selvaraj, "Investigation of chaotic nature of sunspot data by nonlinear analysis techniques", American-Eurasian Journal of Scientific Research **10(5)** (2015) 272. https://doi.org/10.5829/idosi.aejsr.2015.10.5.1150.
[16] Q.-T. Xiao, S.-B. Wang, Z. Zhang & J.-X. Xu, *Analysis of sunspot time series (1749–2014) by means of 0–1 test for chaos detection*, 11th International Conference on Computational Intelligence and Security (2015). https://doi.org/10.1109/CIS.2015.60.
[17] S. T. Ogunjo, A. B. Rabiu, I. A. Fuwape & A. A. Obafaye, "Evolution of dynamical complexities in geospace as captured by Dst over four solar cycles 1964–2008", Journal of Geophysical Research: Space Physics **126** (2021) e2020JA027873. https://doi.org/10.1029/2020JA027873.
[18] C. P. Gonçalves, "Topological machine learning and chaotic attractors decomposition: An application to sunspot chaos", International Journal of Swarm Intelligence and Evolutionary Computation **13** (2024) 387. https://doi.org/10.35248/2090-4908.24.13.387.
[19] F. Takens, "Detecting strange attractors in turbulence", Lecture Notes in Mathematics **898** (1981) 366. https://doi.org/10.1007/BFb0091924.
[20] N. Packard, J. Crutchfield, J. Farmer & R. Shaw, "Geometry from a time series", Physical Review Letters **45** (1980) 712. https://doi.org/10.1103/PhysRevLett.45.712.
[21] A. M. Fraser & H. L. Swinney, "Independent coordinates for strange attractors from mutual information", Physical Review A **33(2)** (1986) 1134. https://doi.org/10.1103/PhysRevA.33.1134.
[22] M. B. Kennel, R. Brown & H. D. I. Abarbanel, "Determining embedding dimension for phase-space reconstruction using a geometrical construction", Physical Review A **45(6)** (1992) 3403. https://doi.org/10.1103/PhysRevA.45.3403.
[23] I. M. Echi, E. V. Tikyaa & B. C. Isikwue, "Dynamics of rainfall and temperature in Makurdi, International", Journal of Science and Research **4(7)** (2015) 493. https://dx.doi.org/10.21275/SUB156176.
[24] P. Grassberger & I. Procaccia, "Characterization of strange attractors", Physical Review Letters **50** (1983) 346. https://doi.org/10.1103/PhysRevLett.50.346.
[25] M. Y. Boon, B. I. Henry, C. M. Suttle & S. J. Dain, "The correlation dimension: A useful objective measure of the transient visual evoked potential?", Journal of Vision **8(1)** (2008) 6. https://doi.org/10.1167/8.1.6.
[26] F. Mitschke & M. Dammig, "Chaos versus noise in experimental data", International Journal of Bifurcation and Chaos **3(3)** (1993) 693. https://doi.org/10.1142/S021812749300060X.
[27] D. Prichard & J. Theiler, "Generating surrogate data for time series with several simultaneously measured variables", Physical Review Letters **73(7)** (1994) 951. https://doi.org/10.1103/PhysRevLett.73.951.
[28] I. M. Echi, E. V. Tikyaa, E. J. Eweh, A. A. Tyovenda & T. Igbawua, "Investigation of the spatial distribution of deterministic chaos in some meteorological variables across Nigeria", African Scientific Reports **4** (2025) 280. https://doi.org/10.46481/asr.2025.4.2.280.

[29] M. Rosenstein, J. J. Collins & C. De Luca, "A practical method for calculating largest Lyapunov exponents from small data sets", Physica D **65** (1993) 117. https://doi.org/10.1016/0167-2789(93)90009-P.
[30] S. M. Pincus, *Approximate entropy as a measure of system complexity*, Proceedings of the National Academy of Sciences **88(6)** (1991) 2297. https://doi.org/10.1073/pnas.88.6.2297.
[31] H. E. Hurst, "Long-term storage capacity of reservoirs", Transactions of the American Society of Civil Engineers **116(1)** (1951) 770. https://doi.org/10.1061/TACEAT.0006518
[32] J. O. Akinsusi, I. A. Fuwape, A. O. Adelakun & S. T. Ogunjo, "Complexity of air temperature along different altitudes of the troposphere over Nigeria", Arabian Journal of Geosciences **16** (2023) 512. https://doi.org/10.1007/s12517-023-11632-6.
[33] R. Kriz, "Finding chaos in Finnish GDP", International Journal of Automation and Computing **11(3)** (2014) 231. https://doi.org/10.1007/s11633-014-0785-6.
[34] G. A. Gottwald & I. Melbourne, "A new test for chaos in deterministic systems", Proceedings of the Royal Society of London A **460** (2004) 603. https://doi.org/10.1098/rspa.2003.1183.
[35] J. Hu, W. W. Tung, J. B. Gao & Y. H. Cao, "Reliability of the 0–1 test for chaos", Physical Review E **72** (2005) 056207. https://doi.org/10.1103/PhysRevE.72.056207.
[36] GFZ Data services, "Geomagnetic and solar indices (Kp, ap, Ap, SN, F10.7)", GFZ Helmholtz Centre for Geosciences, (2025). Available online: https://kp.gfz.de/fileadmin/files_for_gfz_cms/Kp_ap_Ap_SN_F107_since_1932.txt.
[37] G. Adagba, T. Igbawua & E. V. Tikyaa, "Relative roles of cloud, radiative, and solar–geomagnetic processes in modulating convective available potential energy across Nigerian climate zones", ABUAD International Journal of Natural and Applied Sciences (AIJNAS) **5(2)** (2025) 175. https://Doi.Org/10.53982/Aijnas.2025.0502.12-J.
[38] B. W. Joshua, O. M. Oladipo, J. L. Adamu, S. J. Adebiyi & S. O. Ikubanni, "Correlation between sunspot number and geomagnetic storm", Equity Journal of Science and Technology **5(1)** (2018) 157. https://equipost.com/?mno=302644056
[39] M. O. Audu, F. Okeke, E. Tikyaa, T. Jam, P. Onoja & I. Thankgod, "Assessment of seasonal distribution and characterization of geomagnetic storm occurrence during solar cycles 21–24", Indonesian Journal of Earth Sciences **4(1)** (2024) A1035. https://doi.org/10.52562/injoes.2024.1035.
[40] W. Caesarendra, P. Kosasih, K. Tieu & C. Moodie, *An application of nonlinear feature extraction: A case study for low speed slewing bearing condition monitoring and prognosis*, IEEE/ASME International Conference on Advanced Intelligent Mechatronics: Mechatronics for Human Wellbeing, AIM (2013) 1713. https://doi.org/10.1109/AIM.2013.6584344.
[41] M. Dikpati, "The importance of the solar tachocline", Advances in Space Research **38(5)** (2006) 839. https://doi.org/10.1016/j.asr.2005.07.016.
[42] M. Watzke, "3D simulations reveal why the sun flips its magnetic field every 11 years", Smithsonian Story, (2017). Available online: https://www.si.edu/stories/3d-simulations-reveals-why-sun-flips-its-magnetic-field-every-11-years.
[43] C. J. McMahon, J. P. Toomey & D. M. Kane, "Insights on correlation dimension from dynamics mapping of three experimental nonlinear laser systems", PLOS ONE **12(8)** (2017) e0181559. https://doi.org/10.1371/journal.pone.0181559.
[44] S. Motamedi-Fakhr, M. Moshrefi-Torbati, M. Hill, C. M. Hill & P. R. White, "Signal processing techniques applied to human sleep EEG signals: A review", Biomedical Signal Processing and Control **10** (2014) 21. https://doi.org/10.1016/j.bspc.2013.12.003.
[45] V. A. Makarov, R. Muñoz-Arnaiz, O. Herreras & J. Makarova, "Correlation dimension of high-dimensional and high-definition experimental time series Special Collection: Data-Driven Models and Analysis of Complex Systems", Chaos **33** (2023) 1. https://doi.org/10.1063/5.0168400.